Bifunctional Hydrated Gel Electrolyte for Long-Cycling Zn-Ion Battery with NASICON-Type Cathode

Xidong Lin, Guodong Zhou, Jiapeng Liu, Matthew J. Robson, Jing Yu, Yuhao Wang, Zhiqi Zhang, Stephen C. T. Kwok, and Francesco Ciucci*

Aqueous Zn-ion batteries are promising and safe energy storage technologies. However, current aqueous electrolyte Zn-ion battery technology is hindered by undesirable reactions between the electrolyte and electrodes, which can lead to Zn dendrite growth, gas evolution, and cathode degradation. In this study, a hydrated gel electrolyte (HGE) that combines adiponitrile (ADN) and $Zn(ClO_4)_2 \cdot 6H_2O$ in a polymeric framework is created. ADN is found to stabilize the interface between the electrolyte and anode/cathode, enabling smooth Zn stripping/plating and reducing parasitic reactions. The HGE is simple to fabricate, inexpensive, safe, and flexible. Zn/HGE/Zn symmetrical cells can cycle more than 1000 h at 0.5 mA cm^{-2} and 2000 h at 0.2 mA cm^{-2} without short-circuiting, indicating effective suppression of Zn dendrites. Moreover, with a NASICON-type Sr-doped $Na_3V_2(PO_4)_3$ (SNVP) cathode, a Zn/HGE/SNVP full cell can be cycled over 8000 times at 10 C while retaining a high capacity of 90 mAh g^{-1}.

1. Introduction

Aqueous Zn-ion batteries (ZIBs) have been identified as promising energy storage technologies because of their low cost, environmental friendliness, intrinsic safety, and electrochemical characteristics (e.g., high theoretical capacity of 820 mAh g^{-1} and low electrochemical potential of –0.78 V versus the standard hydrogen electrode).[1–4] However, commonly used aqueous electrolytes (AEs), such as 2 M $ZnSO_4$ in water, still limit the development of ZIBs. In fact, water molecules have undesirable surface interactions with both positive and negative electrodes, leading to continuous electrolyte decomposition and electrode degradation. One particular concern is that Zn dendrites can grow uncontrollably on Zn-metal anodes.[5–7] The Zn plating is accompanied by competitive reactions with hydrated electrolyte species, such as the formation of insulating $ZnO/Zn(OH)_2$ and soluble $[Zn(OH)_4]^{2-}$, and the evolution of H_2.[8–11] At the positive electrode, commonly used transition-metal-based materials (e.g., manganese oxide and vanadium oxide) suffer from continuous dissolution of transition-metal ions and structural collapse caused by the insertion of large hydrated cations (e.g., $[Zn(H_2O)_6]^{2+}$ and H_3O^+).[9,12–16]

Various strategies have been developed to alleviate the negative impact of water molecules, including incorporating functional additives or deep eutectic solvents into the electrolyte, and electrode surface modification and alloying.[7,17–19] Recently, "water-in-salt" (WIS), e.g., 20 M lithium bis(trifluoromethanesulfonyl)imide (LiTFSI) and 1 M zinc bis(trifluoromethanesulfonyl)imide (ZnTFSI), have been shown to stabilize AEs.[3,20–22] However, WIS electrolytes are highly toxic and expensive (Figure S1, Supporting Information). Another strategy is to substitute water with organic solvents, including acetonitrile and dimethylformamide.[16,23] However, such organic solvents are highly flammable, which negates the safety advantage of ZIBs. In addition, most inorganic hydrated Zn salts are not soluble in organic solvents.[24] To overcome this challenge, highly soluble but expensive organic imide Zn salts, such as ZnTFSI or zinc trifluoromethanesulfonate (ZnTFMS), need to be used.

In this study, we propose a low-cost hydrated gel electrolyte (HGE), which can effectively reduce the water-derived parasitic reactions at the cathode and anode. The schematic diagram in **Figure 1a** illustrates the preparation of the HGE. A low-cost hydrated salt ($Zn(ClO_4)_2 \cdot 6H_2O$) was dissolved in adiponitrile (ADN), a bifunctional solvent. In order to produce the gel polymer electrolyte, a monomer (poly(ethylene glycol) dimethacrylate (PEGDM)) and an initiator (2-hydroxy-4-(2-hydroxyethoxy)-2-methylpropiophenone) were added. Then, the mixture was polymerized by ultraviolet (UV) curing within a porous polypropylene (PP) scaffold (Figure S2, Supporting Information) to make the flexible HGE. Specifically, poly-PEGDM provides a strong H-bond interaction between the ether group and H_2O, further suppressing water reactivity.[25] PP scaffold can reinforce the gel polymer network. The primary novelty of the

X. Lin, G. Zhou, J. Liu, M. J. Robson, J. Yu, Y. Wang, Z. Zhang,
S. C. T. Kwok, F. Ciucci
Department of Mechanical and Aerospace Engineering
The Hong Kong University of Science and Technology
Hong Kong, Hong Kong SAR, China
E-mail: francesco.ciucci@ust.hk
S. C. T. Kwok
Guangzhou HKUST Fok Ying Tung Research Institute
Guangzhou 511458, China
F. Ciucci
Department of Chemical and Biological Engineering
The Hong Kong University of Science and Technology
Hong Kong, Hong Kong SAR, China

**ADVANCED
SCIENCE NEWS**
www.advancedsciencenews.com

**ADVANCED
FUNCTIONAL
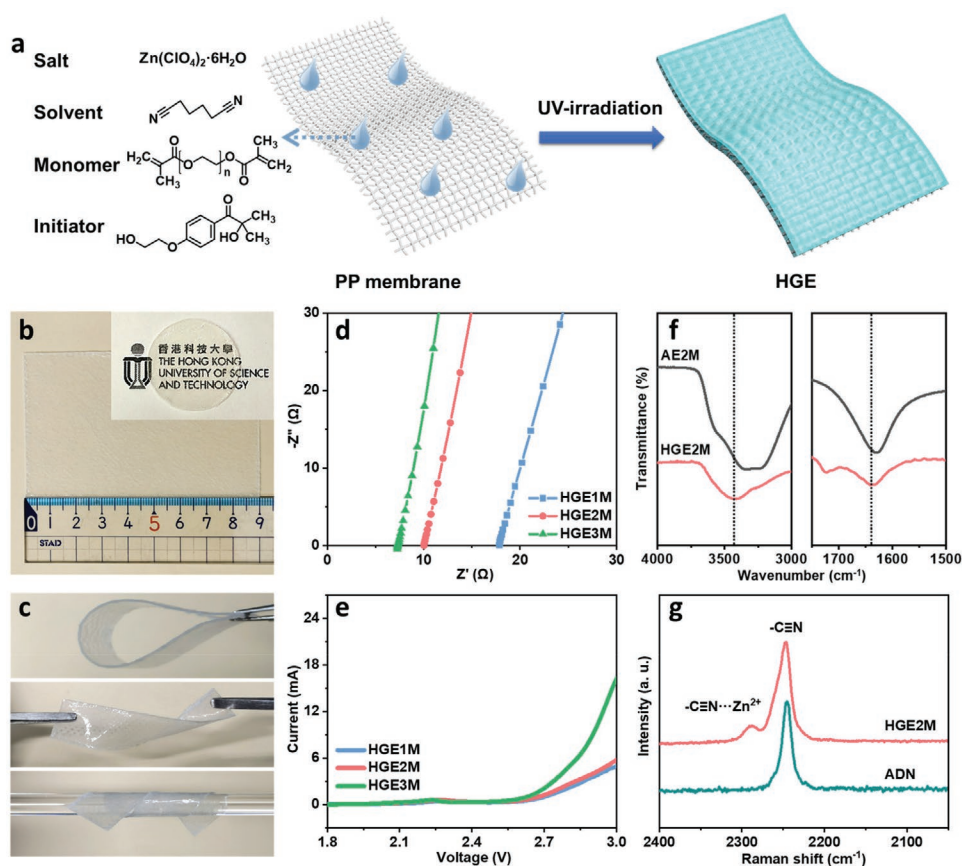MATERIALS**
www.afm-journal.de

Figure 1. a) Schematic illustration of the HGE fabrication process. b) Photograph of a large-scale HGE. c) Photographs of the HGE under bending, twisting, and rolling. d) EIS and e) LSV of the HGE with different salt concentrations. f) FTIR spectra of H-O stretching and H-O bending for HGE2M and AE2M. g) Raman spectra of HGE2M and ADN.

HGE can be summarized as follows: i) Thermally and electrochemically stable ADN was introduced to regulate Zn stripping/plating and form a protective layer on the positive electrode.[26,27] ii) Low-cost and highly soluble $Zn(ClO_4)_2 \cdot 6H_2O$ salt introduces water to the HGE, reducing the viscosity and increasing the conductivity.[7,28] iii) In-depth experimental and theoretical studies were carried out to investigate the stabilization mechanisms of HGE. As a result, HGE is simple to make, low-cost, safe, and flexible. The fabricated Zn/HGE/Zn symmetrical cells could cycle more than 1000 h at 0.5 mA cm^{-2} and 2000 h at 0.2 mA cm^{-2} without short-circuiting, indicating successful Zn dendrite suppression. Moreover, with a NASICON (Na-ion superionic conductor)-type Sr-doped $Na_3V_2(PO_4)_3$ (SNVP) cathode, the Zn/HGE/SNVP full cells exhibited a high specific capacity up to 108 mAh g^{-1} at 0.5 C and long-term cyclic stability up to 8000 cycles at 10 C with a high specific capacity of 90 mAh g^{-1}.

2. Results and Discussion

The HGE is shown in Figure 1b. It could be bent, twisted, and rolled (Figure 1c). Various HGEs were prepared with different concentrations of $Zn(ClO_4)_2 \cdot 6H_2O$. Specifically, HGE with x mol L^{-1} of $Zn(ClO_4)_2 \cdot 6H_2O$ in ADN was denoted as HGExM. The room temperature (RT or 23 °C) ionic conductivities of

HGExM (Figure 1d) were assessed by electrochemical impedance spectroscopy (EIS) using stainless steel (SS)/HGE/SS symmetrical cells. The ionic conductivities of HGExM increased with x. They were 0.77, 1.38, and 1.88 mS cm^{-1} for HGE1M, HGE2M, and HGE3M, respectively. Moreover, linear sweep voltammetry (LSV) was conducted to measure the electrochemical window of the HGExM (Figure 1e). The electrochemical window of HGE narrowed as water content increased as evidenced by oxidation peaks at 2.63, 2.60, and 2.55 V for HGE1M, HGE2M, and HGE3M, respectively. The small oxidative peaks at ≈2.3 V are likely due to the oxidation of free water absorbed by the HGE at the high potential characteristic to the interface between the electrolyte and the positive electrode.[29] HGE2M had relatively high ionic conductivity without compromising high-voltage stability and was, therefore, selected for further electrochemical testing and structural characterization.

The stress–strain curve of HGE2M is shown in Figure S3 (Supporting Information). The Young's modulus, peak stress, and failure strain of HGE2M were 8.5 MPa, 1.0 MPa, and 150%, respectively. The ionic conductivities of HGE2M between −10 and 70 °C are shown in Figure S4 (Supporting Information). The activation energy (E_a) was calculated to be 0.35 eV. We further compared the water-splitting voltage of AE2M (2 mol L^{-1} $Zn(ClO_4)_2 \cdot 6H_2O$ in H_2O) and HGE2M (Figure S5, Supporting Information). For AE2M, H_2/O_2 evolution occurred at a

ADVANCED
SCIENCE NEWS
www.advancedsciencenews.com

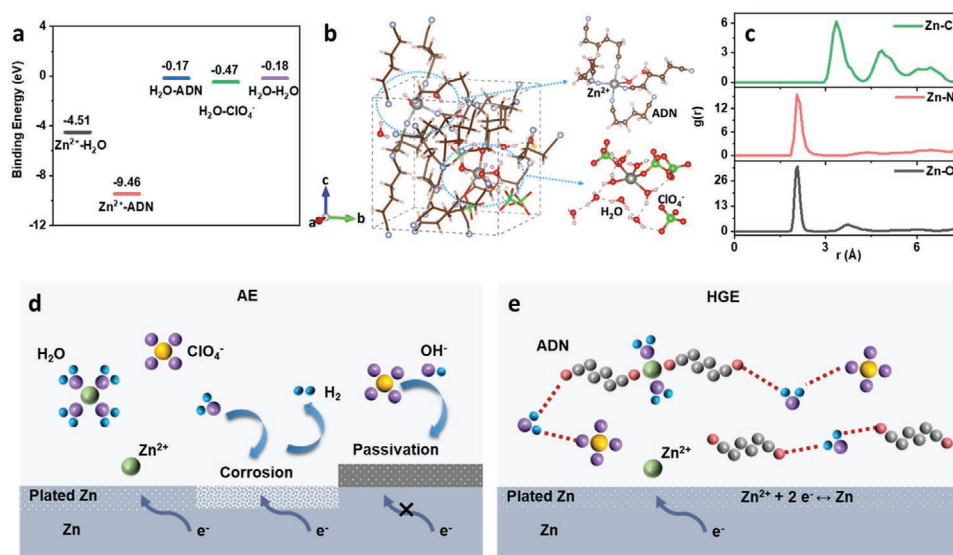**ADVANCED**
FUNCTIONAL
MATERIALS
www.afm-journal.de

Figure 2. a) Binding energies of the major components in HGE2M based on DFT calculation. b) Snapshot of AIMD simulations. c) RDF, g (r), for Zn^{2+}-Cl (ClO_4^-), Zn^{2+}-N (ADN), and Zn^{2+}-O (H_2O) in HGE2M. Schematic illustration of Zn^{2+} solvation structure and corresponding interfacial reactions in d) AE and e) HGE.

higher/lower potential than HGE2M. Furthermore, the measured currents at identical voltages were larger. HGE2M had a larger electrochemical window of −0.13 to 2.60 V, implying effective suppression of water decomposition.

Fourier transform infrared (FTIR) and Raman spectroscopies were used to study the solvation structure of HGE2M and AE2M. In the FTIR spectrum of Figure S6 (Supporting Information), the HGE2M peaks in the 2700–2900 cm^{-1} range could be assigned to the $-CH_2-$ or $-CH_3$ groups in ADN, PP, and Poly-PEGDM. The characteristic peaks of ADN ($-C\equiv N$, 2250 cm^{-1}), Poly-PEGDM ($-C=O$, 1722 cm^{-1}), and ClO_4^- (1083 cm^{-1}) are also shown in Figure S6 (Supporting Information).[30–32] H−O stretching in AE2M was characterized by a broad peak in the range of 3190–3400 cm^{-1}, which indicated the presence of water clusters, see Figure 1f.[25] H−O stretching and bending in HGE2M was at higher wavenumbers than AE2M, suggesting the formation of bound water in the HGE2M network (Figure 1f).[25] Moreover, the Raman spectra suggested the presence of two separated $-C\equiv N$ peaks (Figure 1g): 1) a peak at 2247 cm^{-1} corresponding to free ADN and 2) a peak at 2289 cm^{-1} assigned to bound ADN with Zn^{2+}.[33]

Atomistic simulations were carried out to investigate the coordination environment of the different components in HGE2M and unravel the underpinning stabilization mechanisms. First, the binding energies, E_b, between the pairs of Zn^{2+}-ADN and Zn^{2+}-H_2O were computed to be −9.46 and −4.51 eV by density functional theory (DFT), see **Figure 2a**. These values imply that Zn^{2+} can bind more strongly with ADN than with H_2O. For comparison, the E_b of H_2O–ADN, H_2O–ClO_4^-, and H_2O–H_2O were predicted to be −0.17, −0.47, and −0.18 eV, respectively. These E_b values suggest that ADN and ClO_4^- can also bind with H_2O with moderate strength. Furthermore, ab initio molecular dynamics (AIMD) simulations were performed to identify the solvation structure of Zn^{2+} in HGE2M. A snapshot of an AIMD simulation is shown in Figure 2b. The calculated radial distribution

functions (RDFs), $g(r)$, for Zn^{2+}-Cl (ClO_4^-), Zn^{2+}-N (ADN), and Zn^{2+}-O (H_2O) are given in Figure 2c. In the RDF, a sharp peak at ≈2.1 Å was predicted for both Zn^{2+}-O and Zn^{2+}-N, implying that the Zn^{2+} is coordinated with both H_2O and ADN in its first solvation shell at ≈2 Å. The small peak around 3.8 Å for Zn^{2+}-O suggests that H_2O may also be present in the second solvation shell. By integration of $g(r)$ (described in Figure S7, Supporting Information), the coordination numbers of H_2O and ADN are both found to be 2.5 in the first solvation shell of HGE2M. Consequently, in contrast to the water-rich $Zn(H_2O)_6^{2+}$ solvation structure of the AE, the local configuration of Zn^{2+} in HGE2M is water-deficient.[34,35] The first solvation peak of Zn^{2+}-Cl is located at 3.3 Å, a value farther than that of Zn^{2+}-O and Zn^{2+}-N. The weak interaction between Zn^{2+} and ClO_4^- is ascribed to the high solubility of $Zn(ClO_4)_2 \cdot 6H_2O$ and contributes to the high conductivity of our HGE2M. The Zn^{2+} solvation structures in AE2M and HGE2M are also schematically illustrated in Figure 2d,e. Competitive parasitic reactions in AE will take place in the presence of free hydrated species, e.g., HER, corrosion, and passivation, resulting in the incomplete redox processes of Zn/Zn^{2+}. However, the strong interaction between the H_2O and HGE2M network will significantly reduce the water molecule reactivity and enable smooth Zn stripping/plating.

The Zn/HGE2M/Zn symmetrical cells delivered steady polarization voltages with a long lifespan over 1000 h at 0.5 mA cm^{-2} and 2000 h at 0.2 mA cm^{-2}, see **Figure 3a** and Figure S8 (Supporting Information). In contrast, the Zn/AE2M/Zn cell showed sudden voltage fluctuations after 30 h of cycling at 0.5 mA cm^{-2}. Upon disassembly, scanning electron microscopy (SEM) examination of Zn from a cycled Zn/HGE2M/Zn cell, which we named Zn_{HGE2M}, showed a smooth and dense surface structure (Figure 3b). Such morphological characteristics suggest that HGE2M favors stable and uniform Zn stripping/plating. Conversely, protrusions were observed on Zn_{AE2M}, the Zn from Zn/AE2M/Zn cell (Figure 3c). Moreover,
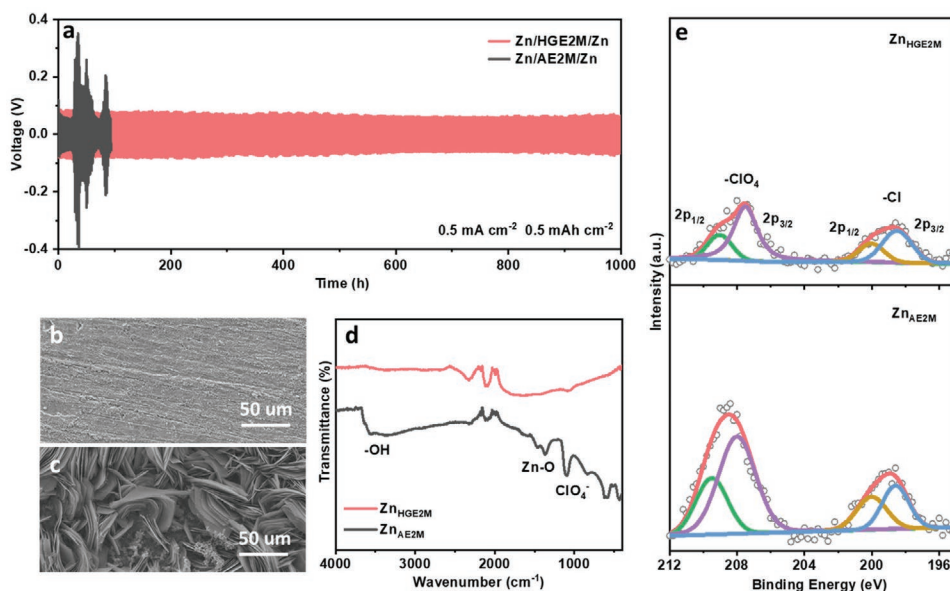
Figure 3. (a) Galvanostatic cycling curves of the symmetrical Zn/Zn cells with HGE2M and AE2M at 0.5 mA cm^{-2} with an areal capacity of 0.5 mAh cm^{-2}. SEM images of the cycled b) Zn_{HGE2M} and c) Zn_{AE2M} electrodes. d) FTIR and e) Cl 2p XPS spectra of the cycled Zn_{HGE2M} and Zn_{AE2M} electrodes.

Zn-O and -OH groups were detected on Zn_{AE2M} via FTIR (Figure 3d), which can be ascribed to water-induced passivation, forming compounds such as ZnO and $Zn(OH)_2$.[36] As shown by X-ray photoelectron spectroscopy (XPS), ADN was absorbed on the surface of the Zn electrode (Figure S9, Supporting Information). Accordingly, we propose that the polar ADN-containing layer can increase the number of nucleation sites and allow homogenous Zn deposition in HGE2M cells.[35,37] Moreover, Cl-containing compounds, which were derived from the reduction of ClO_4^-, were also found on both Zn electrodes.[8,36,38] Measured Cl contents were 0.81 and 1.60 at% for Zn_{HGE2M} and Zn_{AE2M}, respectively. The thin Cl-containing composite layer on Zn_{HGE2M} could shield the interfacial reaction between the Zn electrode and H_2O/ClO_4^-.[8,39,40] However, since the passivating layer derived from ClO_4^- (e.g., $ZnCl_2$) is highly water-soluble, a stable protective layer cannot be obtained on Zn_{AE2M}.[36] Consequently, continuous decomposition of H_2O/ClO_4^- will induce a thick passivating film at Zn/AE2M interface, thus deteriorating the Zn electrode.

NASICON-type materials (e.g., $Na_3V_2(PO_4)_3$ (NVP)) are particularly attractive as Zn ion battery cathodes due to their high voltage platform (>1.2 V vs Zn/Zn^{2+}) and large channels for fast ionic diffusion.[41–45] However, these cathodes suffer from poor rate capability and cyclic stability, due to volumetric change upon intercalation/deintercalation of the large Na$^+$ ion.[46] Previous works have shown that ionic doping (e.g., Al^{3+}, Fe^{3+}, and Mo^{6+}) is an effective strategy for improving NVP electrochemical performance.[47–50] Inspired by this strategy, Sr substitution was used to enhance NVP's structural and electrochemical stability. Since the ionic radius of Sr^{2+} is significantly larger than that of V^{3+} (1.18 vs 0.64 Å), Sr^{2+} can support the crystal lattice, averting collapse due to volume change during Na$^+$ extraction/insertion. Sr substituted NVP at varying Sr-doping concentration was synthesized by solid-state reaction and denoted as SNVPγ (where γ indicates the molar percentage

(mol%) of Sr-doping). The X-ray diffraction (XRD) pattern of the as-prepared SNVPγ is similar to the crystal structure of pure NVP (JCPDS 053-0018), see Figure S10 (Supporting Information). With γ = 1–5 mol% Sr-doping, no impurities could be detected in XRD. However, for SNVP10, $Sr_2P_2O_7$ was produced with a peak appearing at 26.1°. A high-resolution transmission electron microscope (HRTEM) image further confirmed the structure of SNVP5 (**Figure 4a**). The (012) planes lattice fringe of SNVP5 is 6.16 Å (Figure 4b), relative to those of NVP (6.03 Å, Figure S11, Supporting Information).[47] Moreover, a glucose-derived carbonaceous layer could be observed at the surface, which is beneficial to the electronic conductivity. SEM indicated that the SNVP5 powder showed particle diameters ranging from hundreds of nanometers to several micrometers (Figure 4c). Energy-dispersive X-ray spectroscopy (EDS) elemental mappings revealed a homogeneous distribution of Sr, Na, V, P, O, and C elements within SNVP5.

Since the Na$^+$ ion is much larger than Zn^{2+} ion (1.02 vs 0.75 Å), a larger volumetric fluctuation will occur during Na$^+$ extraction/insertion.[51] Therefore, we initially used sodium-ion batteries (SIBs) to evaluate the effect of Sr incorporation and find the most stable SNVPγ product. As shown in Figure S12 (Supporting Information), the capacity and cyclic stability of the SIBs were significantly improved with the increase of Sr content from 0% to 5%. However, the performance of SNVP10 was slightly lower than that of SNVP5. That was because 10% Sr-substitution induced excessive inactive $Sr_2P_2O_7$. As a result, SNVP5 was chosen as cathode material. The Zn storage mechanism in SNVPγ is expected to be similar to undoped NVP and is shown in Figure 4d.[52] Specifically, Na$^+$ ions are extracted from $Na_3V_{1.9}Sr_{0.1}(PO_4)_3$, forming $NaV_{1.9}Sr_{0.1}(PO_4)_3$ during charge. When discharging, Zn^{2+} ions are inserted into $NaV_{1.9}Sr_{0.1}(PO_4)_3$ to form $NaZnV_{1.9}Sr_{0.1}(PO_4)_3$. Subsequently, Zn^{2+} ions will be reversibly extracted from $NaZnV_{1.9}Sr_{0.1}(PO_4)_3$ and inserted into $NaV_{1.9}Sr_{0.1}(PO_4)_3$ during charge and discharge, respectively.[52]
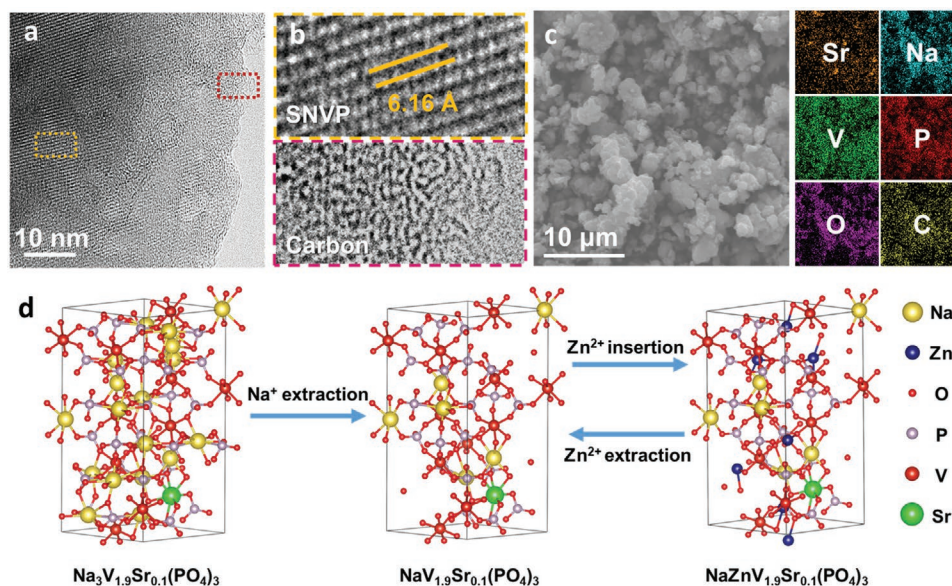
Figure 4. a,b) HRTEM and c) SEM with elemental mapping of SNVP5. Schematic illustration of the charge/discharge process for SNVP.

Figure 5a shows the rate capacities of Zn/HGE2M/SNVP5 from 0.5 to 10 C (1 C = 100 mA g^{-1}). The battery achieved a high reversible specific capacity of 108 mAh g^{-1} at 0.5 C. When further cycled at greater current densities of 1, 2, 3, 5, and 10 C, the specific capacities were 105, 99, 93, 80, and 57 mAh g^{-1}, respectively. When the cell was subsequently cycled at 3 C, the capacity was restored to 92 mAh g^{-1}. The charge/discharge profiles of

Zn/HGE2M/SNVP5 had an operating window between 0.6 and 1.8 V and discharge plateaus over 1.2 V versus Zn/Zn^{2+}, see Figure 5b. The Zn/HGE2M/SNVP5 cells were cycled at 1 and 10 C. Zn/HGE2M/SNVP5 cell exhibited a high specific capacity up to 101 mAh g^{-1} over 400 cycles at 1 C which were higher than that of the NVP cell (68 mAh g^{-1}), see Figure 5c. In contrast, the Zn/AE2M/SNVP5 displayed rapid capacity decay and
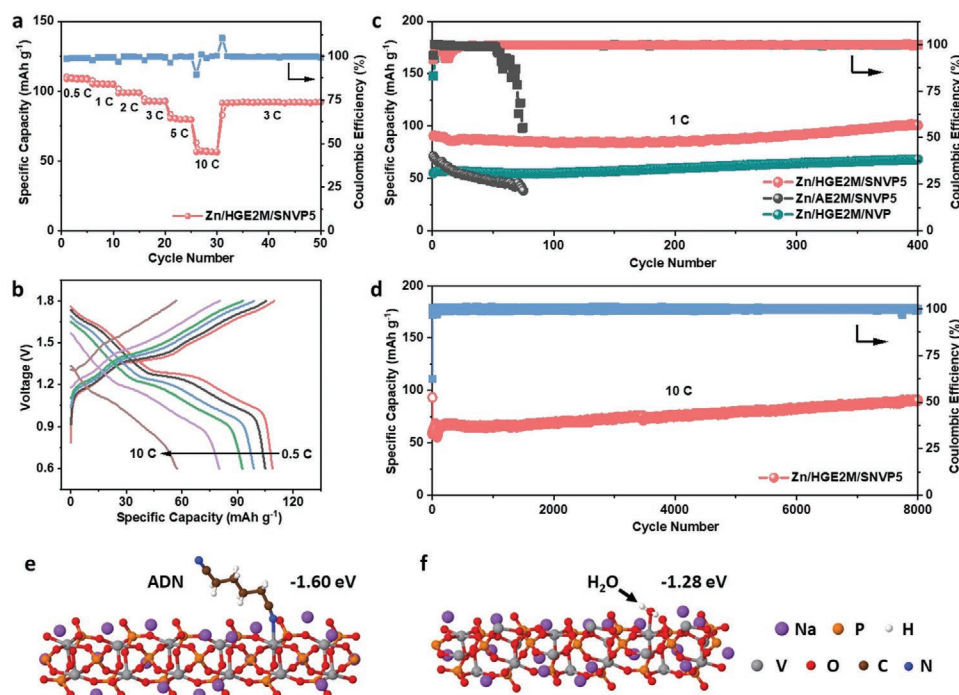

Figure 5. a) Rate performance of Zn/HGE2M/SNVP5 cell (1 C = 100 mA g^{-1}). b) Charge–discharge curves under different rates obtained from Zn/HGE2M/SNVP5 cell. c) Cyclic performance of Zn/HGE2M/SNVP5, Zn/AE2M/SNVP5, and Zn/HGE2M/NVP cells at 1 C. d) Cyclic performance of Zn/HGE2M/SNVP5 at 10 C. Schematic showing adsorption of e) ADN and f) H$_2$O molecules on NVP (012) surface.
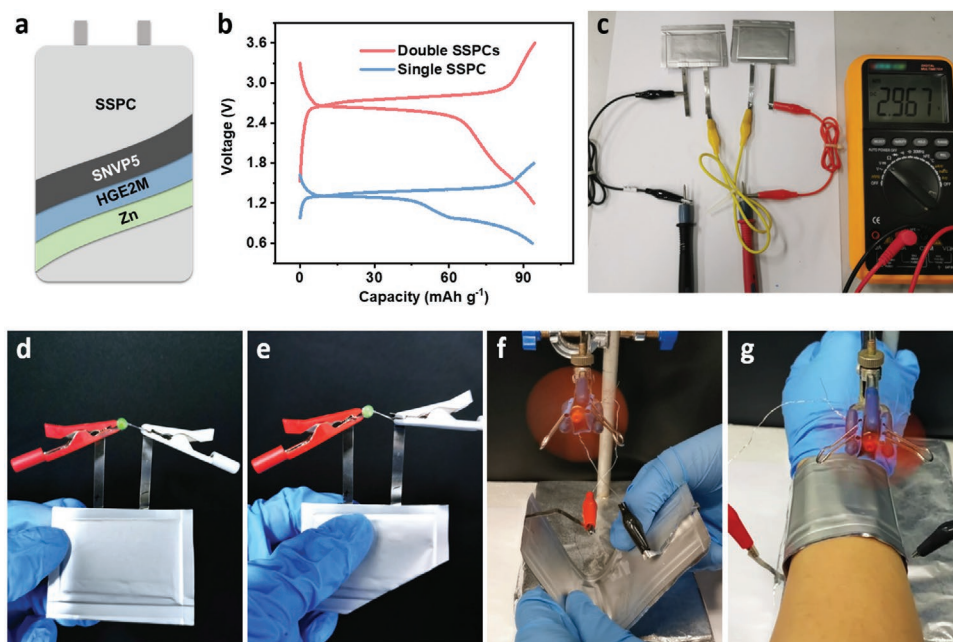
Figure 6. a) Schematic illustration of SSPC. b) Charge–discharge curves of single SSPC and two SSPCs in series. c) Photograph showing the open-circuit voltage of two SSPCs in series. SSPC illuminating an LED bulb d) before and e) after cutting. Photographs of an electric rotor powered by SSPC under f) bending and g) rolling.

ceased to work after 75 cycles. Impressively, when Zn/HGE2M/SNVP5 was cycled at a high current density of 10 C, a reversible capacity of 90 mA g^{-1} could be obtained even after 8000 cycles (Figure 5d). In addition, the high-voltage NASICON cathode, $Na_3V_2(PO_4)_2F_3$ (NVPF), was assembled to evaluate the compatibility of HGE2M. The specific capacities at current densities of 1–10 C are shown in Figure S13a (Supporting Information), and range from 74 to 52 mA g^{-1}. Zn/HGE2M/NVPF were operated at a high cut-off voltage of 2 V versus Zn/Zn^{2+} and had discharge plateaus above 1.6 V versus Zn/Zn^{2+} (Figure S13b, Supporting Information). Zn/HGE2M/NVPF revealed excellent cyclic stability, i.e., 66 mAh g^{-1} at 6 C over 1800 cycles (Figure S13c, Supporting Information). These results surpass recently reported ZIBs with NASICON-type cathodes.[41–44,52–55]

The as-cycled Zn/AE2M/SNVP5 cell showed significant swelling, indicating severe gas evolution (Figure S14, Supporting Information). Conversely, the Zn/HGE2M/SNVP5 cell maintained the same cell thickness after 400 cycles, suggesting strong HER suppression in HGE2M. As shown in Figure S15a (Supporting Information), the separator of a cycled Zn/AE2M/SNVP5 turned green, suggesting the dissolution of the vanadium compounds. Conversely, the cycled HGE2M remained intact (Figure S15b, Supporting Information). XRD and XPS were used to characterize the structure of the cycled SNVP5 cathodes. The XRD results were taken from the Zn/AE2M/SNVP5 and Zn/HGE2M/SNVP5 cells, which were cycled 50 times at 1 C. Comparing with the pristine SNVP5 and SNVP5$_{HGE2M}$ (the SNVP5 from Zn/HGE2M/SNVP5 cell), SNVP5$_{AE2M}$ (the SNVP5 from Zn/AE2M/SNVP5 cell) was seriously degraded with the XRD peaks of the former two cathodes disappearing in SNVP5$_{AE2M}$ (Figure S16, Supporting Information). Moreover, the intensity of V in SNVP5$_{AE2M}$ was much

lower than that of SNVP5$_{HGE2M}$ (Figure S17, Supporting Information).[45] Specifically, the $-C\equiv N$ group was observed in the N 1s spectrum of SNVP5$_{HGE2M}$ (Figure S18, Supporting Information), demonstrating the presence of the ADN layer on the surface of SNVP5$_{HGE2M}$.[27] The adsorption energy (computed by DFT) of ADN molecules (−1.60 eV) on a representative surface (012) of the NVP is lower than that of H_2O (−1.28 eV), implying that the cathode surface was ADN-dominated (Figure 5e,f). The strongly coordinated ADN layer can effectively protect SNVP5 in the HGE2M cell against the corrosion of H_2O.

Solid-state pouch cells (SSPCs) of Zn/HGE2M/SNVP5 were also assembled (**Figure 6a**). As shown in Figure 6b,c, two SSPCs in series could achieve an operational window of 1.2–3.6 V and an output potential to ≈3.0 V. Impressively, the SSPC could illuminate a light-emitting diode (LED) even when cut (Figure 6d,e) with no liquid leakage observed. The flexibility of the solid-state ZIB was also examined, see Figure 6f,g, and Video S1 (Supporting Information). The SSPC was still able to power a rotor even if bent and around a human wrist.

3. Conclusion

A flexible and low-cost HGE was developed for aqueous ZIBs, which showed exceptional compatibility with both ZMA and NASICON-type cathodes. The Zn/HGE2M/Zn symmetrical cells could cycle more than 1000 h at 0.5 mA cm^{-2} and 2000 h at 0.2 mA cm^{-2} without short-circuiting, indicating effective suppression of Zn dendrites. Moreover, the Zn/HGE2M/SNVP5 cell could be cycled over 8000 times at 10 C with a high capacity of 90 mAh g^{-1}. These studies will deliver a new path for the manufacture of safe, low-cost, and scalable AE-based ZIBs.

Supporting Information

Supporting Information is available from the Wiley Online Library or from the author.

Conflict of Interest

The authors declare no conflict of interest.

Data Availability Statement

The data that support the findings of this study are available from the corresponding author upon reasonable request.

[1] H. Pan, Y. Shao, P. Yan, Y. Cheng, K. S. Han, Z. Nie, C. Wang, J. Yang, X. Li, P. Bhattacharya, K. T. Mueller, J. Liu, *Nat. Energy* **2016**, *1*, 16039.

[2] N. Zhang, F. Cheng, Y. Liu, Q. Zhao, K. Lei, C. Chen, X. Liu, J. Chen, *J. Am. Chem. Soc.* **2016**, *138*, 12894.

[3] F. Wang, O. Borodin, T. Gao, X. Fan, W. Sun, F. Han, A. Faraone, J. A. Dura, K. Xu, C. Wang, *Nat. Mater.* **2018**, *17*, 543.

[4] X. Lin, G. Zhou, J. Liu, J. Yu, M. B. Effat, J. Wu, F. Ciucci, *Adv. Energy Mater.* **2020**, *10*, 2001235.

[5] M. Song, H. Tan, D. Chao, H. J. Fan, *Adv. Funct. Mater.* **2018**, *28*, 1802564.

[6] H. Qiu, X. Du, J. Zhao, Y. Wang, J. Ju, Z. Chen, Z. Hu, D. Yan, X. Zhou, G. Cui, *Nat. Commun.* **2019**, *10*, 5374.

[7] J. Zhao, J. Zhang, W. Yang, B. Chen, Z. Zhao, H. Qiu, S. Dong, X. Zhou, G. Cui, L. Chen, *Nano Energy* **2019**, *57*, 625.

[8] L. Wang, Y. Zhang, H. Hu, H. Y. Shi, Y. Song, D. Guo, X. X. Liu, X. Sun, *ACS Appl. Mater. Interfaces* **2019**, *11*, 42000.

[9] C. Xu, B. Li, H. Du, F. Kang, *Angew. Chem., Int. Ed.* **2012**, *51*, 933.

[10] X. Zeng, J. Hao, Z. Wang, J. Mao, Z. Guo, *Energy Storage Mater.* **2019**, *20*, 410.

[11] D. Kundu, S. Hosseini Vajargah, L. Wan, B. Adams, D. Prendergast, L. F. Nazar, *Energy Environ. Sci.* **2018**, *11*, 881.

[12] B. Wu, G. Zhang, M. Yan, T. Xiong, P. He, L. He, X. Xu, L. Mai, *Small* **2018**, *14*, 1703850.

[13] Y. Shen, K. Kordesch, *J. Power Sources* **2000**, *87*, 162.

[14] L. E. Blanc, D. Kundu, L. F. Nazar, *Joule* **2020**, *4*, 771.

[15] L. Zhang, B. Zhang, J. Hu, J. Liu, L. Miao, J. Jiang, *Small Methods* **2021**, *5*, 2100094.

[16] M. Na, Y. Oh, H. R. Byon, *Chem. Mater.* **2020**, *32*, 6990.

[17] W. Xu, K. Zhao, W. Huo, Y. Wang, G. Yao, X. Gu, H. Cheng, L. Mai, C. Hu, X. Wang, *Nano Energy* **2019**, *62*, 275.

[18] L. Kang, M. Cui, F. Jiang, Y. Gao, H. Luo, J. Liu, W. Liang, C. Zhi, *Adv. Energy Mater.* **2018**, *8*, 1801090.

[19] S. B. Wang, Q. Ran, R. Q. Yao, H. Shi, Z. Wen, M. Zhao, X. Y. Lang, Q. Jiang, *Nat. Commun.* **2020**, *11*, 1634.

[20] Y. Zhao, D. Wang, X. Li, Q. Yang, Y. Guo, F. Mo, Q. Li, C. Peng, H. Li, C. Zhi, *Adv. Mater.* **2020**, *32*, 2003070.

[21] L. Zhang, I. A. Rodríguez-Pérez, H. Jiang, C. Zhang, D. P. Leonard, Q. Guo, W. Wang, S. Han, L. Wang, X. Ji, *Adv. Funct. Mater.* **2019**, *29*, 1902653.

[22] C. Zhang, J. Holoubek, X. Wu, A. Daniyar, L. Zhu, C. Chen, D. P. Leonard, I. A. Rodriguez-Perez, J. X. Jiang, C. Fang, X. Ji, *Chem. Commun.* **2018**, *54*, 14097.

[23] M. S. Chae, J. W. Heo, H. H. Kwak, H. Lee, S.-T. Hong, *J. Power Sources* **2017**, *337*, 204.

[24] Z. Ye, Z. Cao, M. O. Lam Chee, P. Dong, P. M. Ajayan, J. Shen, M. Ye, *Energy Storage Mater.* **2020**, *32*, 290.

[25] J. Xie, Z. Liang, Y. C. Lu, *Nat. Mater.* **2020**, *19*, 1006.

[26] X. Lin, J. Yu, M. B. Effat, G. Zhou, M. J. Robson, S. C. T. Kwok, H. Li, S. Zhan, Y. Shang, F. Ciucci, *Adv. Funct. Mater.* **2021**, *31*, 2010261.

[27] S. H. Lee, J. Y. Hwang, S. J. Park, G. T. Park, Y. K. Sun, *Adv. Funct. Mater.* **2019**, *29*, 1902496.

[28] J. Wu, Q. Liang, X. Yu, Q. F. Lü, L. Ma, X. Qin, G. Chen, B. Li, *Adv. Funct. Mater.* **2021**, *31*, 2011102.

[29] S. Kondou, E. Nozaki, S. Terada, M. L. Thomas, K. Ueno, Y. Umebayashi, K. Dokko, M. Watanabe, *J. Phys. Chem. C* **2018**, *122*, 20167.

[30] M. Y. Bhat, N. Yadav, S. A. Hashmi, *ACS Appl. Energy Mater.* **2020**, *3*, 10642.

[31] S. Lin-Gibson, S. Bencherif, J. A. Cooper, S. J. Wetzel, J. M. Antonucci, B. M. Vogel, F. Horkay, N. R. Washburn, *Biomacromolecules* **2004**, *5*, 1280.

[32] Y. Chen, Y.-H. Zhang, L.-J. Zhao, *Phys. Chem. Chem. Phys.* **2004**, *6*, 537.

[33] X. Song, H. He, M. H. Aboonasr Shiraz, H. Zhu, A. Khosrozadeh, J. Liu, *Chem. Commun.* **2021**, *57*, 1246.

[34] T. E. Cooper, D. R. Carl, P. B. Armentrout, *J. Phys. Chem. A* **2009**, *113*, 13727.

[35] Z. Hou, H. Tan, Y. Gao, M. Li, Z. Lu, B. Zhang, *J. Mater. Chem. A* **2020**, *8*, 19367.

[36] W. Yang, X. Du, J. Zhao, Z. Chen, J. Li, J. Xie, Y. Zhang, Z. Cui, Q. Kong, Z. Zhao, C. Wang, Q. Zhang, G. Cui, *Joule* **2020**, *4*, 1557.

[37] Z. Zhao, J. Zhao, Z. Hu, J. Li, J. Li, Y. Zhang, C. Wang, G. Cui, *Energy Environ. Sci.* **2019**, *12*, 1938.

[38] R. Younesi, M. Hahlin, K. Edstrom, *ACS Appl. Mater. Interfaces* **2013**, *5*, 1333.

[39] X. Liang, Q. Pang, I. R. Kochetkov, M. S. Sempere, H. Huang, X. Sun, L. F. Nazar, *Nat. Energy* **2017**, *2*, 17119.

[40] B. Xu, X. Li, C. Yang, Y. Li, N. S. Grundish, P. H. Chien, K. Dong, I. Manke, R. Fang, N. Wu, H. Xu, A. Dolocan, J. B. Goodenough, *J. Am. Chem. Soc.* **2021**, *143*, 6542.

[41] W. Li, K. Wang, S. Cheng, K. Jiang, *Energy Storage Mater.* **2018**, *15*, 14.

[42] G. Li, Z. Yang, Y. Jiang, C. Jin, W. Huang, X. Ding, Y. Huang, *Nano Energy* **2016**, *25*, 211.

[43] G. Li, Z. Yang, Y. Jiang, W. Zhang, Y. Huang, *J. Power Sources* **2016**, *308*, 52.

[44] P. Hu, Z. Zou, X. Sun, D. Wang, J. Ma, Q. Kong, D. Xiao, L. Gu, X. Zhou, J. Zhao, S. Dong, B. He, M. Avdeev, S. Shi, G. Cui, L. Chen, *Adv. Mater.* **2020**, *32*, 1907526.

**ADVANCED
SCIENCE NEWS**

www.advancedsciencenews.com

**ADVANCED
FUNCTIONAL
MATERIALS**

www.afm-journal.de

[45] X. Dong, Y. Lin, P. Li, Y. Ma, J. Huang, D. Bin, Y. Wang, Y. Qi, Y. Xia, *Angew. Chem., Int. Ed. Engl.* **2019**, *58*, 5623.

[46] Y. Chen, J. Cheng, C. Wang, Z. He, Y. Wang, D. Li, L. Guo, *Chem. Eng. J.* **2021**, *413*.

[47] X. Li, Y. Huang, J. Wang, L. Miao, Y. Li, Y. Liu, Y. Qiu, C. Fang, J. Han, Y. Huang, *J. Mater. Chem. A* **2018**, *6*, 1390.

[48] J. Y. Park, Y. Shim, Y.-i. Kim, Y. Choi, H. J. Lee, J. Park, J. E. Wang, Y. Lee, J. H. Chang, K. Yim, C. W. Ahn, C.-W. Lee, D. K. Kim, J. M. Yuk, *J. Mater. Chem. A* **2020**, *8*, 20436.

[49] Y. Chen, Y. Xu, X. Sun, C. Wang, *J. Power Sources* **2018**, *375*, 82.

[50] H. Li, X. Yu, Y. Bai, F. Wu, C. Wu, L.-Y. Liu, X.-Q. Yang, *J. Mater. Chem. A* **2015**, *3*, 9578.

[51] B. Tang, L. Shan, S. Liang, J. Zhou, *Energy Environ. Sci.* **2019**, *12*, 3288.

[52] P. Hu, T. Zhu, X. Wang, X. Zhou, X. Wei, X. Yao, W. Luo, C. Shi, K. A. Owusu, L. Zhou, L. Mai, *Nano Energy* **2019**, *58*, 492.

[53] J. S. Ko, P. P. Paul, G. Wan, N. Seitzman, R. H. DeBlock, B. S. Dunn, M. F. Toney, J. N. Weker, *Chem. Mater.* **2020**, *32*, 3028.

[54] X. Zhang, H. Chen, W. Liu, N. Xiao, Q. Zhang, X. Rui, S. Huang, *Chem. Asian J.* **2020**, *15*, 1430.

[55] W. Li, X. Jing, K. Jiang, D. Wang, *ACS Appl. Energy Mater.* **2021**, *4*, 2797.